/N-20

330277

TECHNICAL MEMORANDUM
X - 75

EXPERIMENTAL AND ANALYTICAL STUDY OF

ROLLING-VELOCITY AMPLIFICATION DURING THE THRUSTING

PROCESS FOR TWO 10-INCH-DIAMETER SPHERICAL

ROCKET MOTORS IN FREE FLIGHT

By C. William Martz and Robert L. Swain

Langley Research Center
Langley Field, Va.

NATIONAL AERONAUTICS AND SPACE ADMINISTRATION

WASHINGTON

September 1959
Declassified March 18, 1960

NATIONAL AERONAUTICS AND SPACE ADMINISTRATION

TECHNICAL MEMORANDUM X-75

EXPERIMENTAL AND ANALYTICAL STUDY OF

ROLLING-VELOCITY AMPLIFICATION DURING THE THRUSTING

PROCESS FOR TWO 10-INCH-DIAMETER SPHERICAL

ROCKET MOTORS IN FREE FLIGHT*

By C. William Martz and Robert L. Swain

SUMMARY

Two 10-inch-diameter spherical rocket motors have been flight tested at the NASA Wallops Station. These tests were conducted to measure "spin-up" or amplification of the spinning velocity of the motor during the thrusting process due to internal swirling of the exhaust gases. Model 1, a heavy-wall motor, experienced an increase in spin rate during thrusting of about 10 percent, whereas model 2, a flight-type motor with a lightweight motor case, experienced an increase of about 19 percent. The propellant weight and geometry were the same for both motors. A simple relationship for "spin-up" which satisfies these measured results is reported herein. Both models were spin stabilized throughout their flights.

A theoretical method of predicting spin-up was derived and used to extend the measured 10-inch-motor results to spherical rocket motors of other sizes having a similar propellant geometry. This method is presented and its predictions are shown to compare favorably with the measured flight results.

INTRODUCTION

High-speed vehicles traveling within the earth's atmosphere usually are restricted to slender shapes because of drag considerations. However, as rocket-powered vehicles reach higher and higher altitudes where the air is very thin, aerodynamic drag loses its influence on their design. Consequently, for drag-free operation some designers have turned

*Title, Unclassified.

to spherical rocket motors which, by virtue of their highly efficient pressure-vessel properties, tend to give optimum rocket performance by means of high mass ratios. A comprehensive account of the early development of a 10-inch-diameter spherical rocket motor by the Langley Pilotless Aircraft Research Division is given in reference 1.

At these high altitudes, one method of maintaining a constant pitch and yaw attitude of the vehicle is by spin stabilization where the vehicle is made to spin about a principal axis usually coincident with the thrust axis. During the preliminary design of a high-altitude vehicle, it was the combination of spin stabilization and spherical rocket motors which called attention to the problem of how the spinning velocity of a spherical rocket motor would be affected by internal gas flow while the motor was thrusting. It was known that the propellant geometry would retard the swirling of the gases within the motor and that this would result in angular momentum being transferred from the propellant to the motor case with an "inflow turbine" effect. The extent of this effect was not known.

Since several factors in the thrusting process for a spherical rocket motor were unknown, such as the path of the propellant gases within the motor to the nozzle and propellant erosion, it was decided to determine this "spin-up" effect experimentally. Two spin-stabilized 10-inch-diameter spherical rocket motors were ground launched for this purpose and the experimental results were extended analytically to spherical motors of various other sizes having a similar propellant geometry.

This paper presents the flight history of spinning velocity for both spherical rocket-powered vehicles and compares the results with the predictions of a limited theoretical analysis which is given in the appendix. A chart showing theoretical spin-up for any size of spherical motor is included also.

SYMBOLS

I_E	roll inertia of empty model, slug-ft^2
I_L	roll inertia of model loaded with propellant, slug-ft^2
p	model rolling velocity, radians/sec
p_E	model rolling velocity immediately after thrusting
p_L	model rolling velocity at ignition

MODELS AND EQUIPMENT

Models

Each model used in this investigation consisted of a 10-inch-diameter spherical rocket motor equipped with a spinsonde to provide a means of obtaining a history of spinning velocity during the flight. The overall dimensions of these models are shown in figure 1. Photographs of the models are shown in figure 2. Both rocket motors had identical internal ballistic configurations, corresponding to that presented in reference 1, and were loaded with T-22, a polysulfide-ammonium perchlorate propellant. Design chamber pressure was 600 lb/sq in.

The motor of model 1 was that used in the early development of spherical rocket motors at Langley. Its history includes three successful static ground tests. The motor case was designed for strength and reusability with little concern for weight. Construction details for this motor are reported in reference 1.

The motor of model 2 was designed for flight use, and its construction details are shown in figure 3. The case weight was minimized by welding the hemispherical sections together and machining the nozzle integral with the case. The ratio of loaded weight to empty weight for this motor was 10.3. This mass ratio does not include the spinsonde and equatorial band (shown in fig. 1) which was added for this particular test to increase the spin inertia of the motor case and thereby prevent the possibility of excessive spin-up with consequent high spin rates and structural failure.

Values of weight, center-of-gravity location, and moment of inertia in roll and pitch are presented for both models in table I for both loaded and empty conditions.

No attempt was made to balance these models either statically or dynamically. However, moment-of-inertia measurements by swinging as a simple pendulum about various transverse axes revealed no measurable unbalance for either model.

Other Equipment

Both models were ground launched from the NASA Wallops Station at an elevation angle of 75°. The launcher used for these models is shown in figure 4. Each model was fitted into a bucket which prevented wobble during the preflight spinning. A nozzle blowout diaphragm prevented premature separation of the model from the bucket. At launching, the

bucket and model were spun at about 1,200 rpm by the electric motor shown mounted on the launcher. Ignition of the rocket motor was accomplished through slip rings mounted on the spindle supporting the bucket. Exhaust gases were voided through holes in the bucket and through the hollow launcher spindle.

A Rawin set AN/GMD-1A recorded atmospheric data at all flight altitudes. Flight-path data were obtained from tracking radar, and a CW Doppler velocimeter was used to determine flight velocity. Visual flight records were obtained by photography.

PREFLIGHT TESTS

Previous to the flight tests of models 1 and 2, a ground test was conducted to measure the spin-up of the 10-inch-diameter motor ultimately used as model 1. The motor was mounted on ball bearings in a test stand with freedom to spin about its thrust axis. The motor was spun to 600 rpm before firing by directing flows of compressed air into small buckets mounted on the periphery of the rig encasing the rocket motor. Upon ignition of the propellant, several of the bolts holding the motor hemispheres failed and the case parted. A propellant leakage between the motor hemispheres during propellant casting was believed to be responsible for the failure of the motor. Although the motor case was undamaged, this type of test was not repeated because of equipment damage and because of the considerable difficulty experienced in obtaining a consistent calibration of the bearing friction under simulated thrust loads. It was decided instead to avoid this trouble by measuring spin-up in a free-flight test which would at the same time provide an excellent opportunity to evaluate the spherical rocket motor under actual flight conditions.

A lightweight 10-inch-diameter spherical rocket motor, identical to that of model 2 except for a longer, nonthreaded nozzle, was fired statically on the ground to measure thrust output. The measured thrust-time curve, along with a calculated pressure-time history, is presented in figure 5. It should be mentioned that during this test the diffuser section of the nozzle burned off just before the normal end of thrusting.

RESULTS AND DISCUSSION

Spin Stability

An important byproduct of this spin-up investigation was the opportunity to check qualitatively the preflight assumptions and calculations regarding spin stabilization of these models. Motion pictures of both

flights were obtained with various cameras at different locations and indicated that these models were dynamically stable at least to the peak of their trajectories which is about the maximum range of the cameras for these sized objects. The motion pictures did show an expected slight wobbling motion of the models during the initial part of both flights. Another unplanned and most fortunate result of the spinning action occurred during the launching of model 1 and is described in the next section entitled "Ignition."

Ignition

Ignition of solid-propellant rocket motors has long been an art rather than a science. Previous static tests indicated that ignition delay or "hangfire" was a problem area. Accordingly, the igniter for model 1 was made considerably more powerful than would normally have been used and contained 50 grams of U.S. Flare 2A boron pellets in a frangible plastic tube. However, during the flight test, ignition of the propellant was delayed $1\frac{1}{2}$ seconds. During this time the impulse of the igniter pushed the spinning model about 8 feet into the air after which the model settled back to earth and spun like a top until the propellant ignited. The model then relaunched to a trajectory not much different than that planned. The performance of the model throughout the remainder of the flight seemed to be unaffected by this occurrence, and the gyroscopic stability induced by the spinning saved the test from being a failure.

The igniter for model 2 was increased to 55 grams of pellets, the maximum amount that could be contained in the plastic tube. During the flight test of model 2, a 1-second hangfire occurred. As model 2 was considerably lighter in weight than model 1, it was projected about 15 feet into the air by the igniter impulse. It did not sink more than half a foot before the propellant ignited and thrusted the model into its anticipated trajectory.

As reported in reference 1, a mercury wash is employed as a part of the manufacturing process of spherical rocket motors. Later ignition tests at Langley have shown that the residual mercury in the propellant after the washing process has a pronounced effect on delaying propellant ignition. This problem has been overcome by thorough sanding of the propellant surface.

Performance

After the launching both models appeared to function satisfactorily in that the velocity histories and flight-path results were about as

expected. Low-altitude launching of these vehicles resulted in high drag which limited the maximum flight Mach number of models 1 and 2 to 1.12 and 1.15, respectively. This kept the models at close range which allowed better photographic coverage of the flights. Motion pictures of the flight indicate that the nozzle of model 2 burned out near the end of the thrust period. This was expected because of the similar result previously mentioned with regard to the static ground test of an identical motor. More important was the fact that the lightweight flight motor had performed under flight conditions while spin stabilized.

Momentum Transfer

The increase in spin rate during burning of the propellant is shown in figures 6(a) and 6(b) for models 1 and 2, respectively. For model 1, the spin rate at launching was determined from motion pictures as the spinsonde data were not available until the model attained some altitude.

The faired values of figure 6 indicate an increase in spin rate during thrusting of about 10 percent for model 1 and of about 19 percent for model 2. The difference in these results is attributed mainly to the different ratio of roll inertia before thrusting to roll inertia after thrusting for each model. Consider the following momentum equation which pertains to both models:

$$\begin{pmatrix} \text{Angular-roll} \\ \text{momentum, loaded} \end{pmatrix} = \begin{pmatrix} \text{Angular-roll} \\ \text{momentum, empty} \end{pmatrix} + \begin{pmatrix} \text{Angular-roll-} \\ \text{momentum loss} \\ \text{through nozzle} \end{pmatrix} \quad (1a)$$

which can be expressed as

$$I_L p_L = I_E p_E + \text{Loss} \quad (1b)$$

from which

$$\frac{p_E}{p_L} = \frac{I_L}{I_E}\left(1 - \frac{\text{Loss}}{I_L p_L}\right) \quad (2)$$

Now, in order to apply equation (2), it is necessary to evaluate the "loss." It is logical that this loss must be related to the total amount of transferable momentum (i.e., the momentum of the unburned propellant). When the loss per unit of transferable momentum was found to be nearly constant for models 1 and 2 (89 percent and 88 percent, respectively), the average value of 88.5 percent was used as a basis of correlating the spin-up results of the two models as follows:

$$\frac{\text{Loss}}{\text{Transferable momentum}} = \frac{I_L p_L - I_E p_E}{(I_L - I_E)p_L} = 0.885 \tag{3}$$

for which

$$\frac{p_E}{p_L} = 0.115 \frac{I_L}{I_E} + 0.885 \tag{4}$$

This simple relationship satisfies the measured results of the two models reported herein. However, these motors were the same size, had about the same rolling velocity, and were not greatly different with respect to the inertia parameter I_L/I_E. Since other applications of spherical rocket motors of various sizes with widely varying inertia ratios and different spin requirements are of interest, it was deemed important to attempt a limited theoretical analysis of the spin-up. This was done and is presented in the appendix. This analysis indicates that "spin-up" is a mixture of several variables and is strongly influenced by propellant geometry. The main factors which result in greater spin-up are a larger ratio of roll inertia before and after thrusting and higher values of initial spinning velocity.

Theoretical spinning-velocity histories were calculated with this theory for the two models of the present investigation and can be seen in figure 6. External roll damping was considered negligible in this application. The calculated curves are seen to approximate the experimental results very well. Although the theoretical values appear slightly high, it is estimated that they are actually slightly low when the effects of external spin damping are taken into consideration.

Figure 7 is a summary plot of theoretical spin-up for any size of spherical motor having the internal geometry considered in the appendix. For this geometry, spin-up is seen to be a function of only two variables: the ratio of rolling inertia before and after thrusting and the tangential velocity at the motor equator when the thrusting starts.

By considering larger or smaller spherical rocket motors with similar propellant geometry, with the same ratio of roll inertia before thrusting to after thrusting, and with initial spin rates consistent with spin stabilization requirements (where spin rate required varies inversely with scale factor), the theoretical analysis indicates that the ratio of rolling velocity before thrusting to that after thrusting will be the same for all sized motors.

CONCLUDING REMARKS

"Spin-up" or amplification of the spinning velocity of a rocket motor during the thrusting process due to internal swirling of the exhaust gases has been demonstrated in the flight tests of two 10-inch-diameter spherical rocket motors. Model 1, a heavy-wall motor, experienced an increase in spin rate during thrusting of about 10 percent, whereas model 2, a lightweight flight motor, experienced an increase of about 19 percent. A simple relationship for spin-up was obtained to correlate these results.

A theoretical method for predicting spin-up has been derived and used to extend the measured 10-inch-motor results to spherical rocket motors of other sizes having a similar propellant geometry. This method is presented and its predictions are shown to compare favorably with the measured flight results.

Langley Research Center,
    National Aeronautics and Space Administration,
        Langley Field, Va., July 1, 1959.

APPENDIX

THEORETICAL MOMENTUM TRANSFER IN SPHERICAL

ROCKET MOTORS DURING THRUSTING

The method described herein is intended to yield approximate pre-
dictions of the spin history of spherical rocket motors during burning
of the propellant and to show which variables are of importance during
the process. The analysis but not the method is restricted to a given
propellant geometry which has been found practical in use.

The distribution of the propellant charge is described in detail in
reference 1 and can best be described as a circular arrangement of seven
spherical wedges or "melon slices" within a "thick" spherical shell. A
quartered view of a six-segment motor mock-up is shown in figure 8.

Although the experimental motors had tapered separator spaces (slots
or channels between the wedges) with flanged peripheries, the theoretical
geometry was simplified somewhat by assuming the separator spaces to be
flat plates. This is indicated in figures 9 and 10.

The burning of the propellant was assumed to take place in six steps
or layers of equal thickness which are shown in figure 9. In all cal-
culations involving these steps, the half-burned geometry of each layer
was used.

In a nonspinning motor, the gases formed during the burning of the
propellant flow inward and rearward along the slots and finally out of
the nozzle with no rotary motion about the motor longitudinal axis. How-
ever, for a spinning motor, the gases formed during the burning also have
a swirling motion about the motor spin axis and with respect to the
rotating motor. This motion is caused by the conservation of angular
momentum of the gas particles and results in some of the particles col-
liding with the unburned propellant and transferring part of their angu-
lar momentum to the motor before leaving the nozzle. Other particles,
because of their initial location along the walls of the slots, are able
to swirl out of the motor without touching the propellant and without
losing any of their angular momentum to the motor. This method approxi-
mates spin-up of the motor by determining how much of the original angu-
lar momentum is retained by the motor during the thrusting process. In
application, the method is rather lengthy for hand calculation but is
readily adapted to be carried out on a digital computer.

10

The following symbols are used in the appendix:

A   cross-sectional area of seven slots in planes parallel to motor spin axis (variable with y), $14b l_2 \sin \phi$

b   width of slot for nth step, $\frac{n}{2} - 0.050$

d_1 depth of slot at ball center, $l_2 - l_1 \cos \frac{360}{14}$

d_2 depth of slot in zone q, $l_2 \cos \gamma_q - l_2 + d_1$

E   mean fraction of step mass in momentum transfer zone for step n

E_q fraction of step mass in momentum transfer zone for zone q and step n

I_n total roll inertia of motor after burning of step n

I_{n-1} total roll inertia of motor before burning of step n

k   mean radius of gyration of step n mass not in momentum transfer zone

l_1 distance from motor longitudinal axis to propellant peaks for nth step, $\frac{b}{2} \csc \frac{360}{14}$

l_2 perpendicular distance from motor center to floor of slots at ball center, $3.375 + \frac{n}{4}$

m   particle mass

n   burning step, 1 to 6

p   motor spinning velocity about longitudinal axis

p_n motor rolling velocity after burning of step n

p_{n-1} motor rolling velocity before burning of step n

q   longitudinal slot zones, 1 to 5

R   radius

r   distance from particle path to model roll axis

r_o initial radius of particle path,

$$\sqrt{\left(l_2 - y_{initial}\right)^2 + \left(x_{initial} - \frac{b}{2}\right)^2}$$

S   surface burning area of that part of all seven slots from $y = 0$ to any particular value of y,

$$7\left[l_2^2(2\phi - \sin 2\phi) + 2l_2 b\phi\right]$$

$S_{d,1}$ value of S at $y = d_1$

S_q slot-surface area in zone q, $\frac{14}{5}\left(l_2 \sin \phi_{d,1}\right)\left(b + 2d_2\right)$

Δt variable time increment used in iteration process of determining particle tracks

Δt_e effective burning time of motor

V_T tangential particle velocity about motor longitudinal axis with respect to an axis system rotating with the model

V_x velocity of particle in x-direction (respect to motor)

V_y velocity of particle in y-direction (respect to motor)

v   inward velocity of slot gas flow (in y-direction) for a nonspinning motor, in./sec

$v_{d,1}$ value of v at $y = d_1$

W   propellant weight

ΔW weight of propellant burned during step n

x,y   particle slot coordinates (see fig. 11)

x_{L_q}, y_{L_q} initial x,y coordinates of particle track which just intersects adjacent peak of unburned charge in zone q

$$\gamma_q = \sin^{-1}\left(\frac{2q - 1}{10}\sin\phi_{d,1}\right)$$

ρ gas density in motor, 0.00022 lb/cu in.

$$\phi = \cos^{-1}\left(1 - \frac{y}{l_2}\right)$$

$\phi_{d,1}$ value of ϕ at $y = d_1$, $\cos^{-1}\left(1 - \dfrac{d_1}{l_2}\right)$

Subscript:

N   Nth step of iteration process for determining particle tracks

The momentum equation governing the spin-up process is expressed as

$$\begin{pmatrix}\text{Model rolling}\\ \text{momentum before}\\ \text{burning of step } n\end{pmatrix} = \begin{pmatrix}\text{Model rolling}\\ \text{momentum after}\\ \text{burning of step } n\end{pmatrix} + \begin{pmatrix}\text{Rolling-momentum}\\ \text{losses during}\\ \text{burning of step } n\end{pmatrix}$$

or

$$I_{n-1}P_{n-1} = I_n P_n + \text{Losses}$$

In order to determine the losses which occur during the burning of step n, it is necessary to approximate the internal flow pattern of the gases during this step. Since the flow takes place in the slots between the propellant wedges, the geometry of these slots should be examined. Figures 11 and 12 show a typical slot ($n = 3$) in which slot depth is seen to vary with location along the longitudinal axis of the motor. The total length of each slot was broken into five equally spaced q zones on each side of the symmetry line as indicated in figure 12. Sections of the same slot ($n = 3$) taken perpendicular to the model longitudinal axis are shown in figure 13 for $q = 1$, 3, and 5. The width of the slot b is constant for all values of q.

A possible flow pattern was developed to conform with the following assumptions: The slot flow takes place in planes perpendicular to the motor longitudinal axis, and the gas particles act independently of each other. Although it is certain that these assumptions are not entirely correct, they offer a simplified means of attacking the problem and, it is believed, do not affect the results substantially.

Consider the slot section of $q = 1$ in figure 13. Under the afore-mentioned assumptions the flow is in the plane of the paper. The flow pattern is established by a step-by-step integration of the particle paths from the two velocities v and V_T. The flow velocity in the y-direction for a nonspinning motor v was assumed constant across the slot and was computed from mass-flow requirements as follows:

$$v = \frac{W}{\Delta t_e} \frac{1}{\rho} \frac{1}{S_{d,1}} \frac{S}{A}$$

where

$$\frac{S}{A} = \frac{l_2^2(2\phi - \sin 2\phi) + 2bl_2\phi}{2bl_2 \sin \phi}$$

with

$$\cos \phi = 1 - \frac{y}{l_2}$$

Thus, under the aforementioned assumptions, v depends only on n and y.

The symbol V_T denotes the tangential velocity of the flow parti-cles about the motor longitudinal axis and with respect to the rotating motor. Its value is determined by equating the initial particle momentum about the roll axis (with respect to a nonrolling motor axis system) to the particle momentum at any point in its path within the slot. Referring to figure 13 gives

$$mr_0^2 p = mr^2 \frac{V_T + rp}{r}$$

which can be expressed as

$$V_T = \frac{r_0^2 p}{r} - rp$$

and also gives

$$V_y = v + V_T \frac{x - \frac{b}{2}}{r} = v + p \frac{x - \frac{b}{2}}{r^2}\left(r_0^2 - r^2\right)$$

14

and

$$V_x = V_T \frac{l_2 - y}{r} = p \frac{l_2 - y}{r^2} \left(r_o^2 - r^2\right)$$

Since

$$x = x_{initial} + \int V_x \, dt$$

and

$$y = y_{initial} + \int V_y \, dt$$

the step-by-step evaluation is

$$x_N = x_{N-1} + \frac{p_{n-1}\left(l_2 - y_{N-1}\right)\Delta t}{\left(l_2 - y_{N-1}\right)^2 + \left(x_{N-1} - \frac{b}{2}\right)^2}\left[r_o^2 - \left(l_2 - y_{N-1}\right)^2 - \left(x_{N-1} - \frac{b}{2}\right)^2\right]$$

and

$$y_N = y_{N-1} + \Delta t \left\{ v_{N-1} + \frac{p_{n-1}\left(x_{N-1} - \frac{b}{2}\right)}{\left(l_2 - y_{N-1}\right)^2 + \left(x_{N-1} - \frac{b}{2}\right)^2}\left[r_o^2 - \left(l_2 - y_{N-1}\right)^2 \right.\right.$$

$$\left.\left. - \left(x_{N-1} - \frac{b}{2}\right)^2\right]\right\}$$

where

$$r_o^2 = \left(l_2 - y_{initial}\right)^2 + \left(x_{initial} - \frac{b}{2}\right)^2$$

The particle paths are computed from these equations for different initial locations as shown in figure 14 for $q = 1$ and $n = 3$. By interpolating between these various paths, the limiting particle path is found in which the particle just intersects the adjacent propellant peak at the top of the slot. Examples of these limiting paths are shown in figure 13.

It is now reasoned that all particles having paths "above" the limiting path represent a complete momentum loss since, under previous assumptions, they cannot transfer any of their momentum. This loss is given by the term

$$(1 - E)\Delta W k^2 \frac{p_n + p_{n-1}}{2}$$

where

$$k^2 = \frac{1}{\displaystyle\sum_{q=1}^{5}\left(d_1 - y_{L_q} + x_{L_q}\right)}\left\{\sum_{q=1}^{5}\left[\left(l_2^2 + \frac{b^2}{4}\right)\left(d_1 - y_{L_q}\right) - l_2\left(d_1^2 - y_{L_q}^2\right)\right.\right.$$

$$\left.\left. + \frac{1}{3}\left(d_1^2 - y_{L_q}^3\right) + x_{L_q}\left(l_2 - d_1^2 + d_2\right)^2 + x_{L_q}\left(\frac{b}{2}\right)^2 - \frac{b}{2}x_{L_q}^2 + \frac{1}{3}x_{L_q}^3\right]\right\}$$

the fraction of step mass "under" limiting particle track, E, is

$$E = \frac{\displaystyle\sum_{q=1}^{5} E_q S_q}{\displaystyle\sum_{q=1}^{5} S_q}$$

and

$$E_q = 1 - \frac{d_1 + x_{L_q} - y_{L_q}}{2d_2 + b}$$

Consider now all particles having paths under the limiting particle path. These particles are assumed to flow to the adjacent sidewall and then out of the slot along this wall. Thus, their momenta would be transferred into the remaining motor mass except for that momentum which the particles possess upon separation from the slot. The remaining

particle momentum upon leaving the slot then represents the following momentum loss to the process (see fig. 13):

$$E \; \Delta W l_1{}^2 \frac{p_n + p_{n-1}}{2} + E \; \Delta W l_1{}^2 \frac{v_{d,1}}{2 l_1{}^2}$$

Writing the momentum equation in full gives

$$I_{n-1} p_{n-1} = I_n p_n + E \; \Delta W l_1{}^2 \left(\frac{p_n + p_{n-1}}{2} + \frac{v_{d,1}{}^b}{2 l_1{}^2} \right) + (1 - E) \Delta W k^2 \frac{p_n + p_{n-1}}{2}$$

from which the following spin-up equation is obtained:

$$\frac{p_n}{p_{n-1}} = \frac{I_{n-1} - \frac{E}{2} \Delta W l_1{}^2 \left(1 + \frac{v_{d,1}{}^b}{l_1{}^2 p_{n-1}} \right) - \frac{1 - E}{2} \Delta W k^2}{I_n + \frac{E}{2} \Delta W l_1{}^2 + \frac{1 - E}{2} \Delta W k^2}$$

This equation was evaluated for both models of the present investigation by using integrated values of inertia and weight increment based upon the propellant distribution assumed for the analysis. (See fig. 15.) Results are shown in figure 6 and are discussed in the "Results and Discussion" section. After it was realized that the integrated effects of the spin-up equation could be expressed as a function of only two variables for any size of spherical motor having the propellant geometry herein considered, a summary plot was prepared for prediction purposes and is presented in figure 7. The variables used are the roll-inertia ratio before and after thrusting and the tangential velocity at the motor equator when thrusting starts.

By considering larger or smaller spherical rocket motors with a similar propellant geometry, with the same ratio of roll inertia before and after thrusting, and with initial spin rates consistent with spin-stabilization requirements (where spin rate required varies inversely with scale factor), the analysis indicates that the ratio of rolling velocity before and after thrusting will be the same for all sized motors.

REFERENCE

1. Thibodaux, Joseph G., Jr., Swain, Robert L., and Wright, George:
     Analytical and Experimental Studies of Spherical Solid-Propellant
   Rocket Motors.   NACA RM L57G12a, 1957.

18

TABLE I

DYNAMICAL CONSTANTS OF ROCKET MOTORS

Constant	Model 1		Model 2	
	Loaded	Empty	Loaded	Empty[a]
Weight, lb	48.90	18.88	38.45	8.55
Center-of-gravity station	15.21	15.10	15.01	14.23
Model roll inertia, slug-ft^2 . .	0.1412	0.0747	0.1082	0.0417
Model pitch inertia, slug-ft^2 . .	0.1638	0.0952	0.1194	0.0518

[a]Indirectly measured or calculated because of method of manufacture.
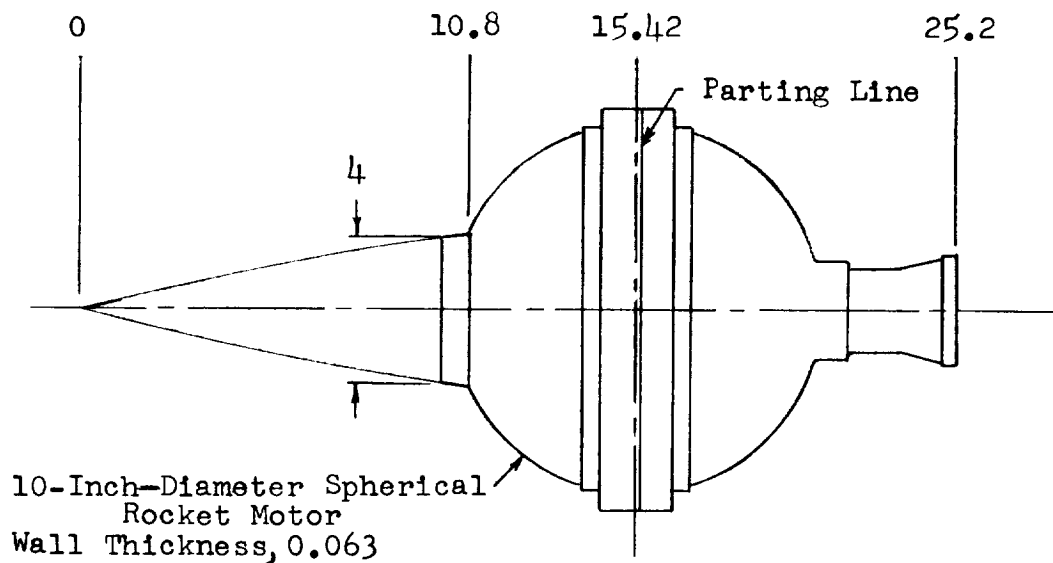
(a) Model 1.
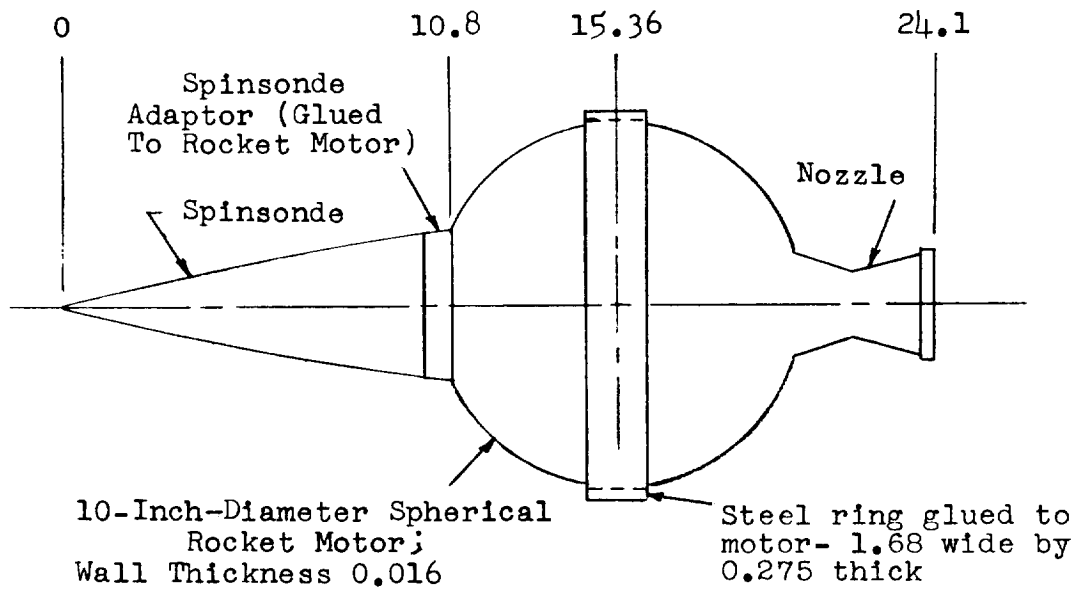
(b) Model 2.

Figure 1.- Sketch of models. All dimensions are in inches.

20

(a) Model 2; side view.   L-58-2907

Figure 2.- Spherical rocket motor with attached spinsonde.
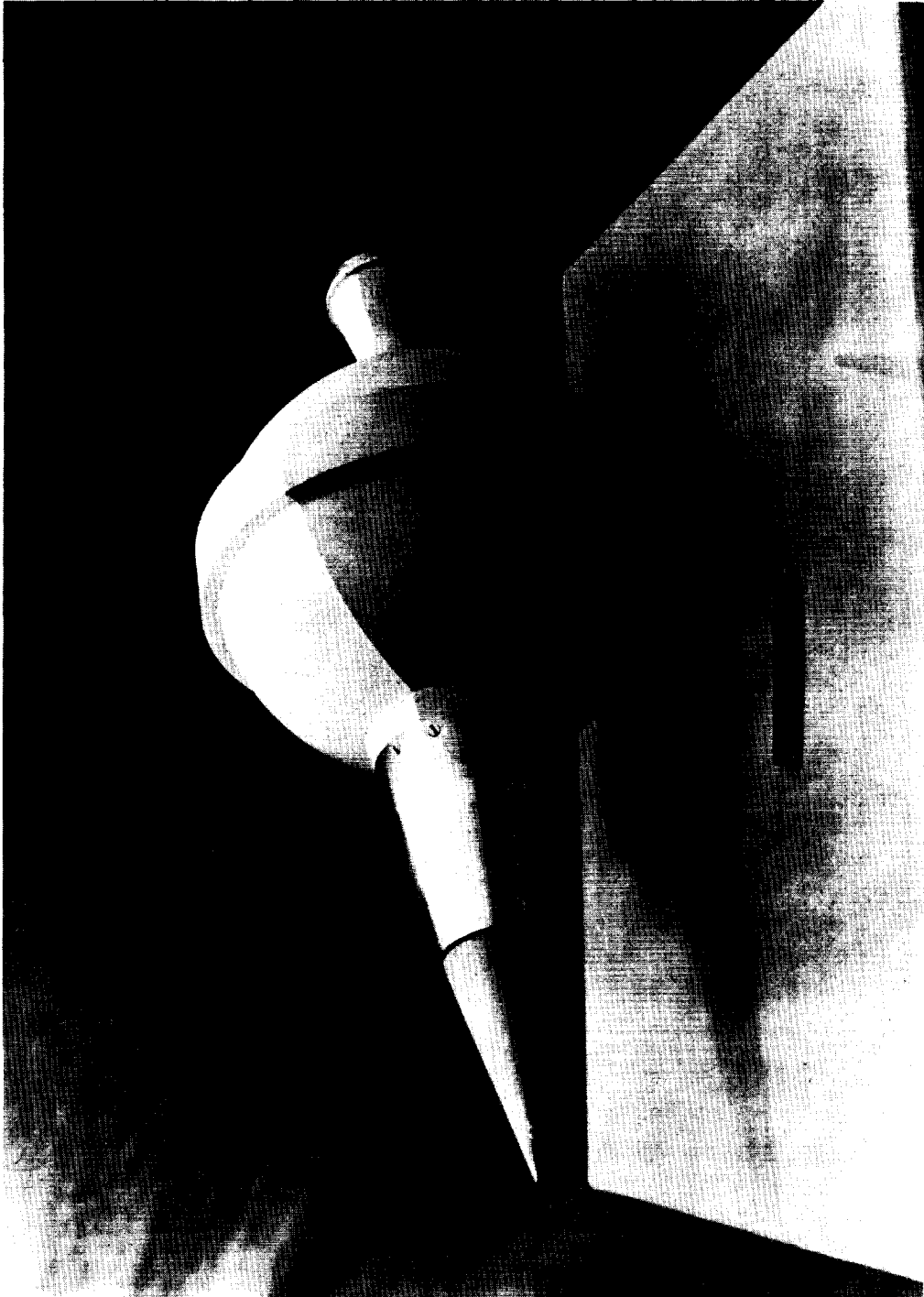
L-58-2908

(b) Model 2; front view.

Figure 2.- Continued.
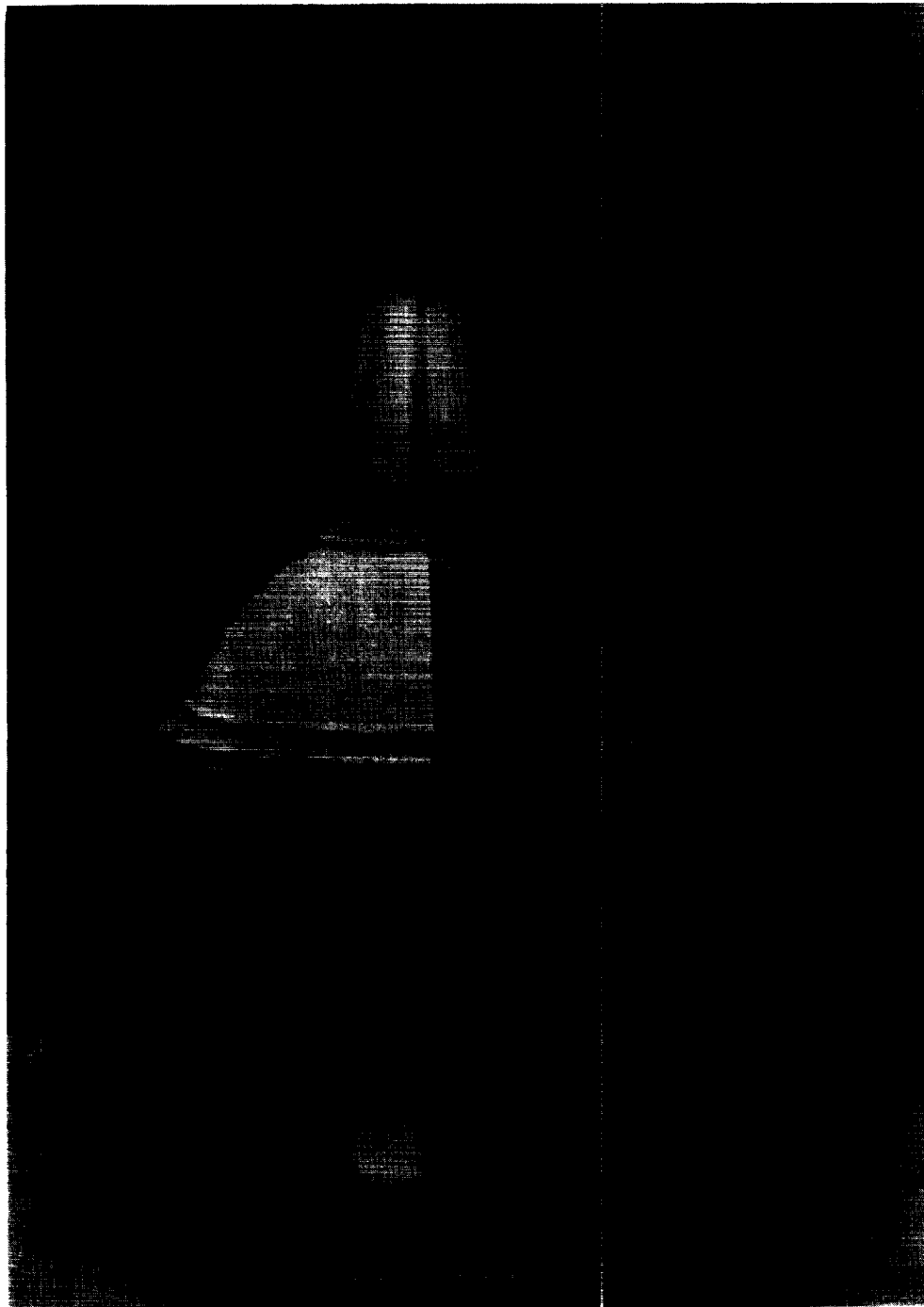
(c) Model 1; side view.   L-58-2909

Figure 2.- Concluded.

Nozzle dimensions:
Throat diameter- 1.442 inches
Exit diameter- 2.829 inches
Half-angle- 15°

AGX graphite insert

0.015 phenopreg liner

5-Inch Spherical Radius

0.015 wall;
SAE 8630 steel
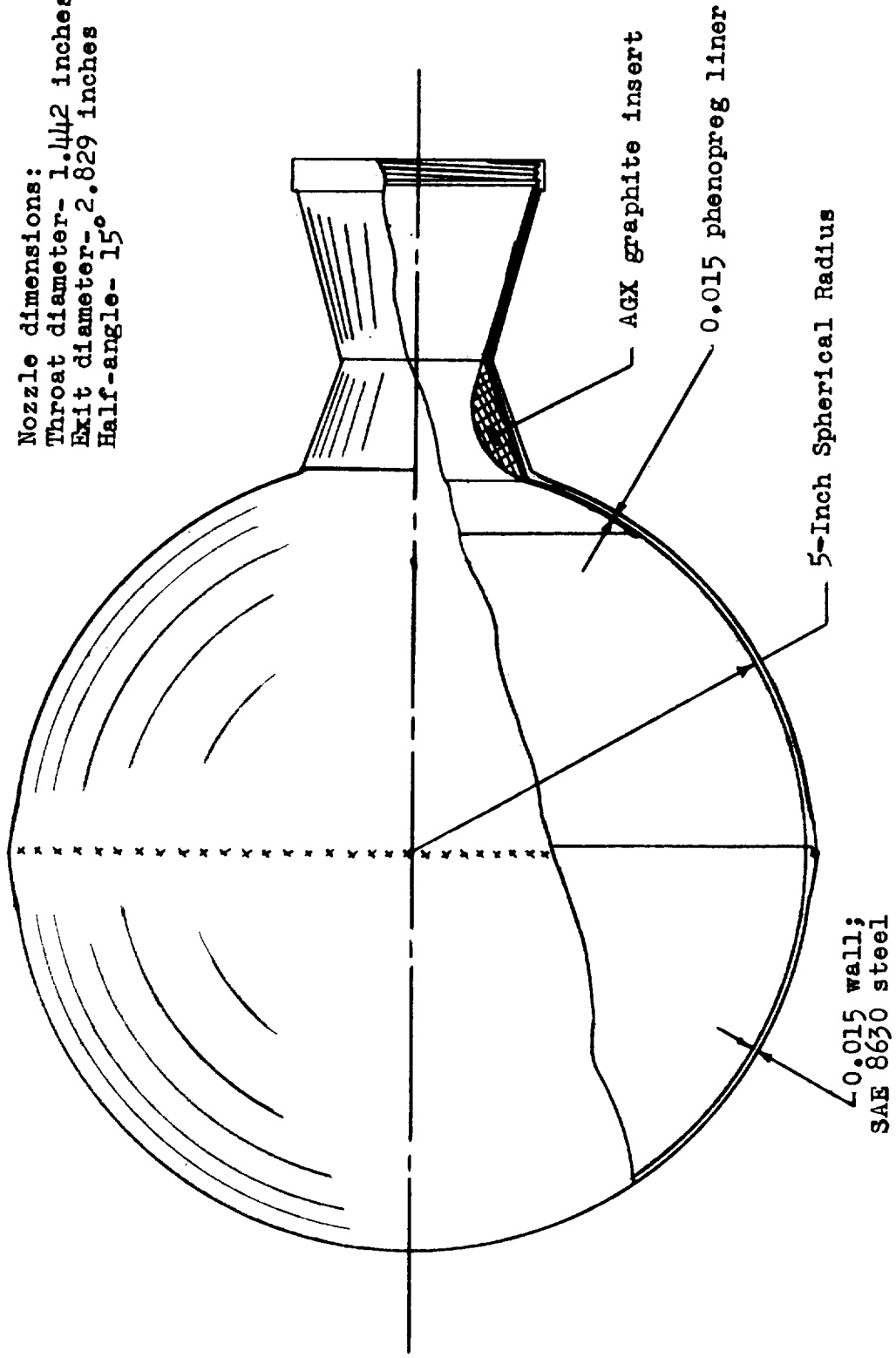
Figure 3.- The 10-inch-diameter spherical-rocket flight case. All dimensions are in inches unless otherwise specified.
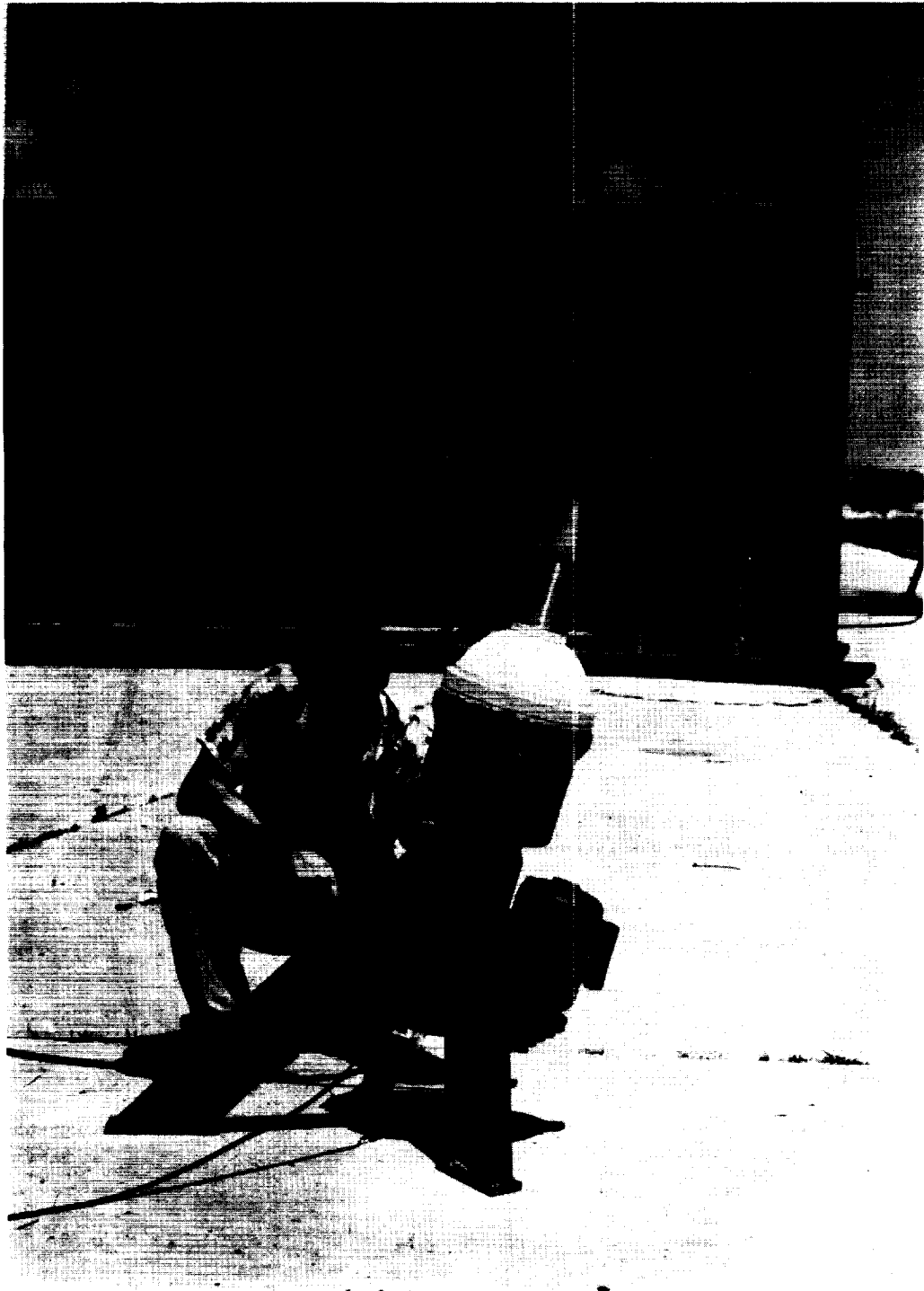
Figure 4.- Model 1 shown on launcher.   L-58-3247.1
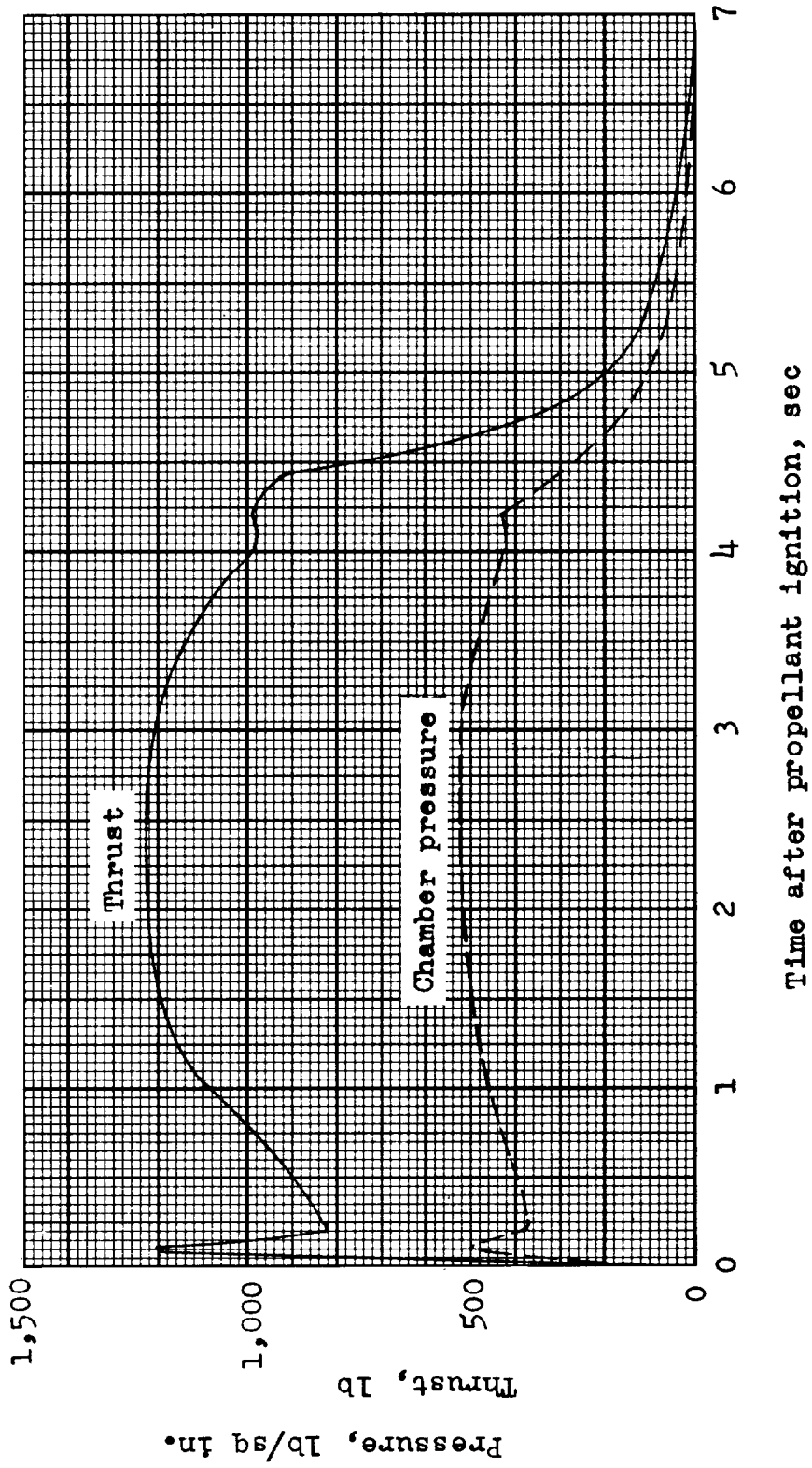
Figure 5.- Typical time history of thrust and pressure for static test of flight-type 10-inch-diameter spherical rocket motor.
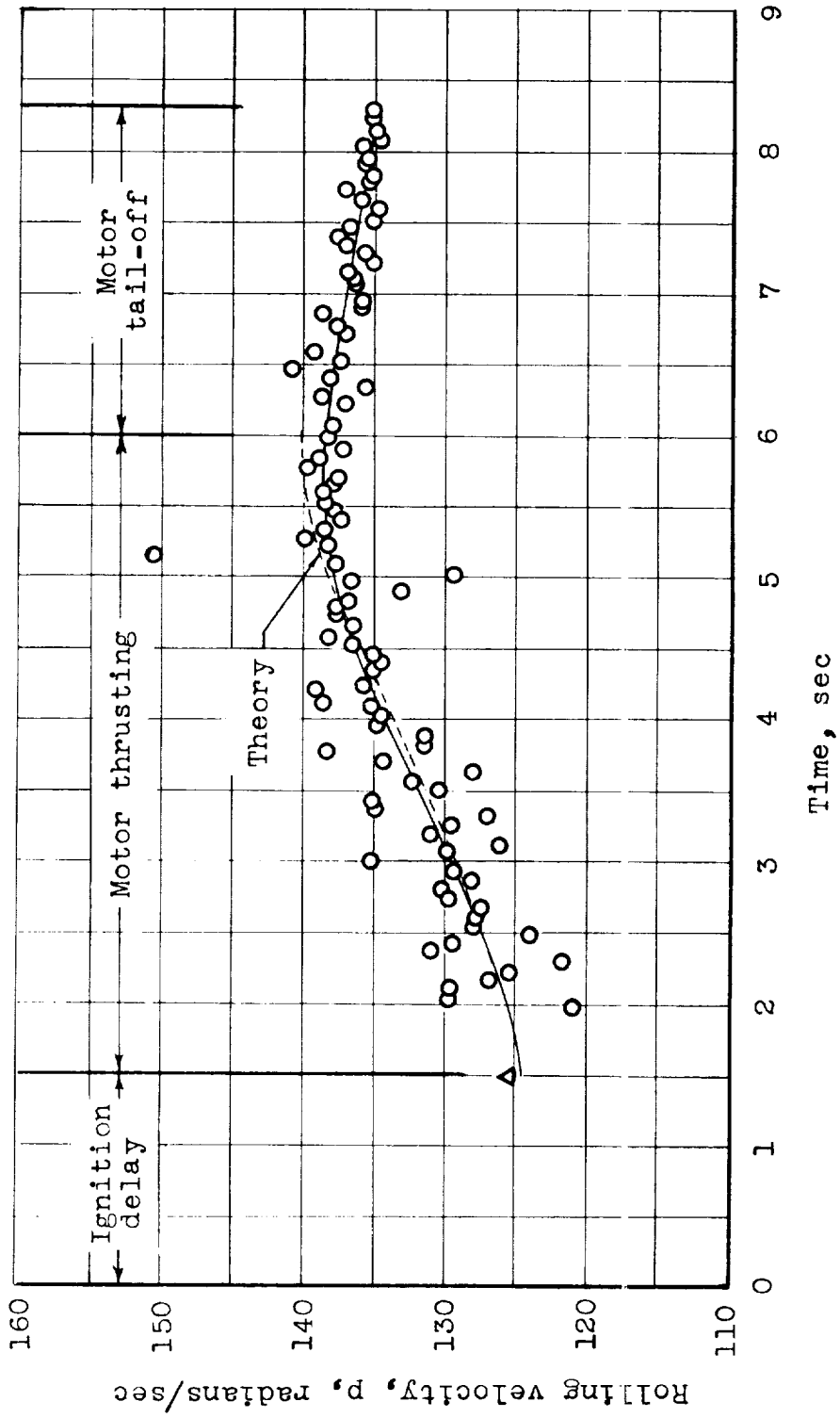
Figure 6.- Experimental and theoretical time histories of rolling velocity.

(a) Model 1.
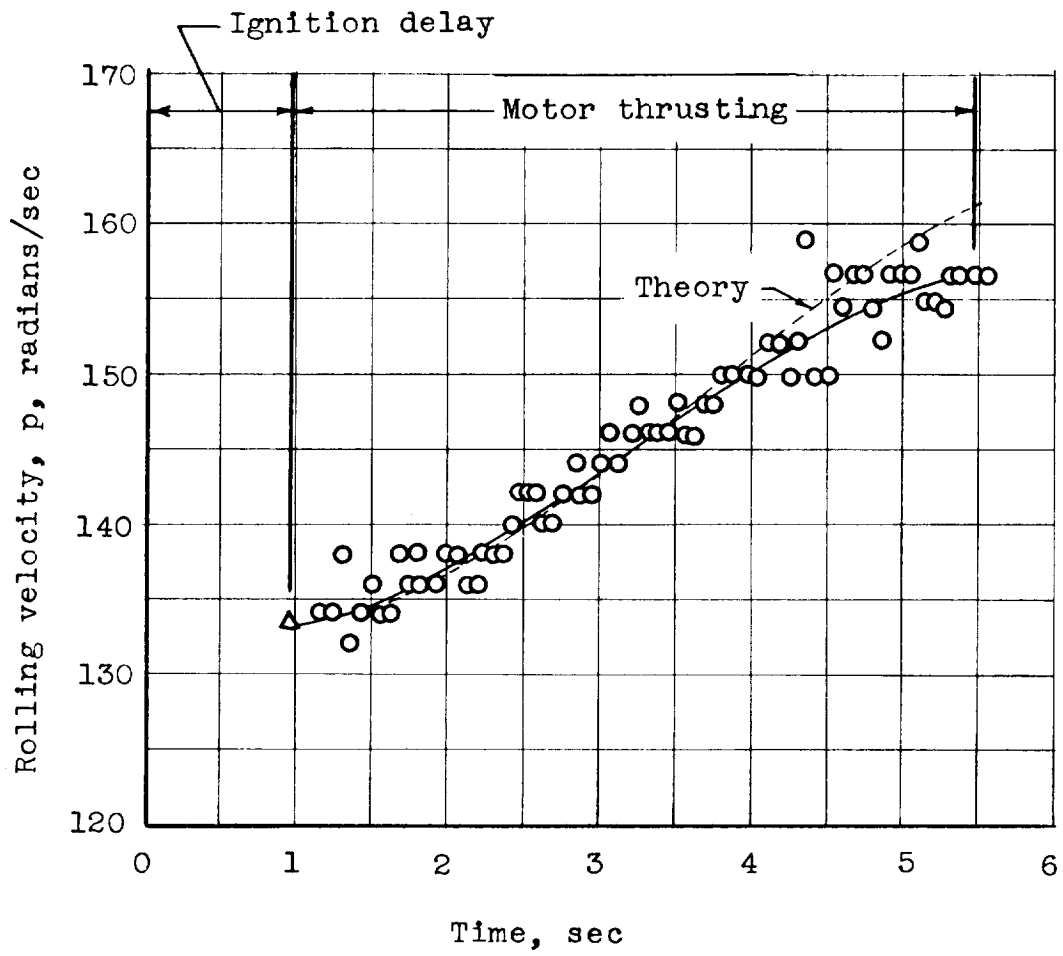
(b) Model 2.

Figure 6.- Concluded.
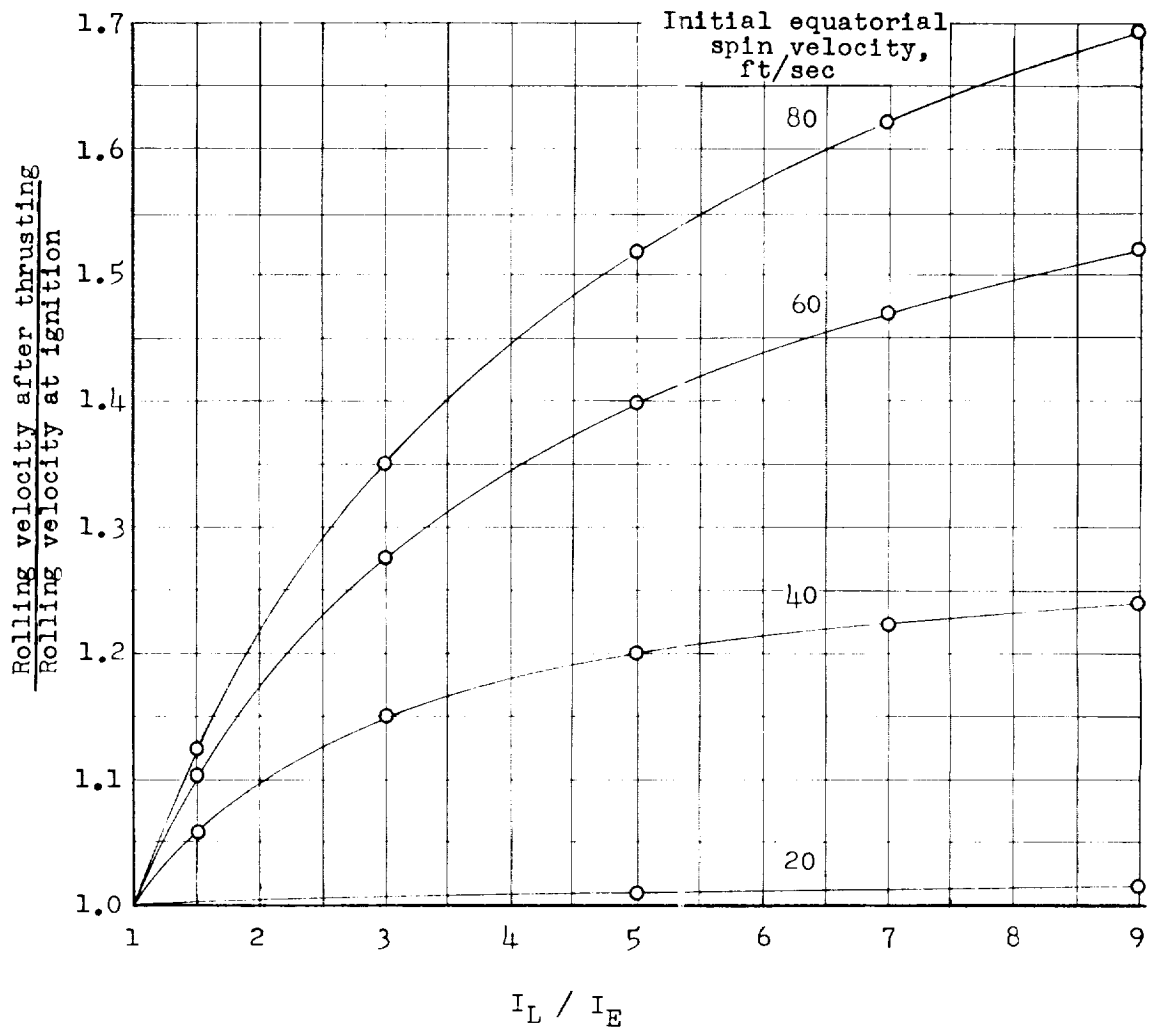
Figure 7.- Chart for determining theoretical spin-up of spherical rocket motors having a described propellant geometry.
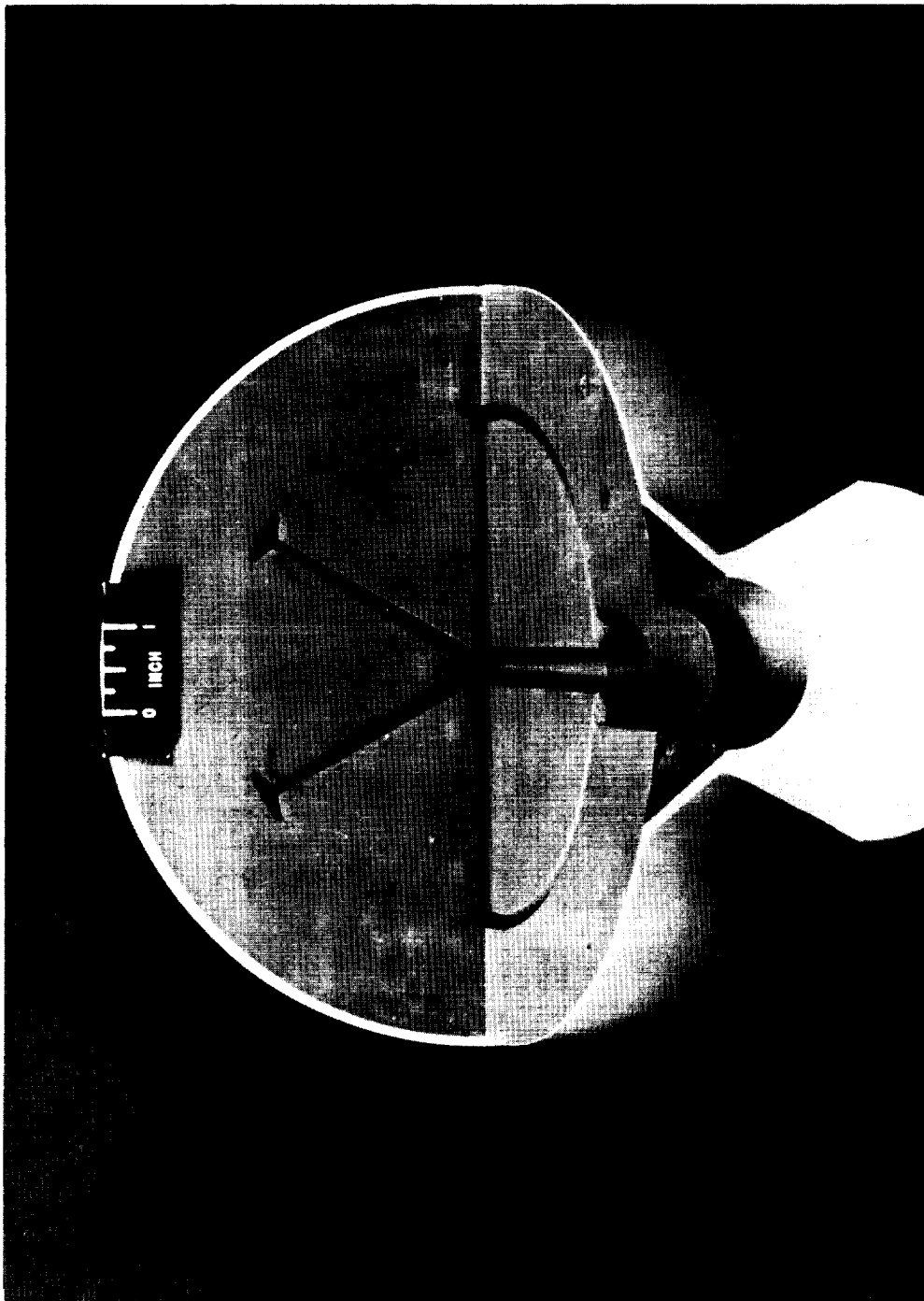
Figure 8.- Cutaway view of six-segment spherical rocket-motor mock-up showing port cavity configuration.
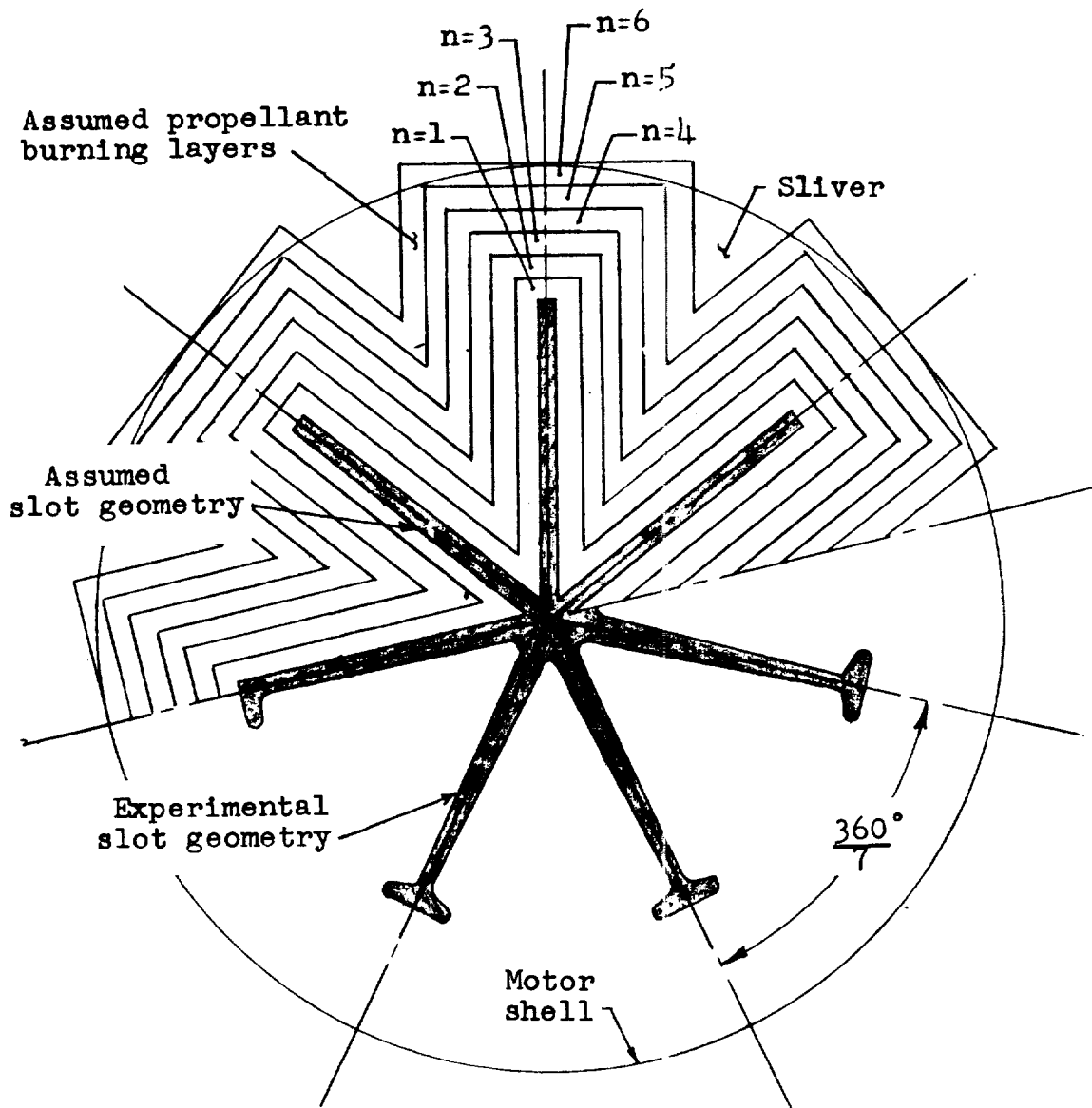
Figure 9.- Full axial section at sphere center showing actual and assumed slot geometry. Burning layers assumed for spin-up analysis shown.

.25

360°
7

.375 R

.094 R

.063 R

.05 R

.20

.15

.65

3.5
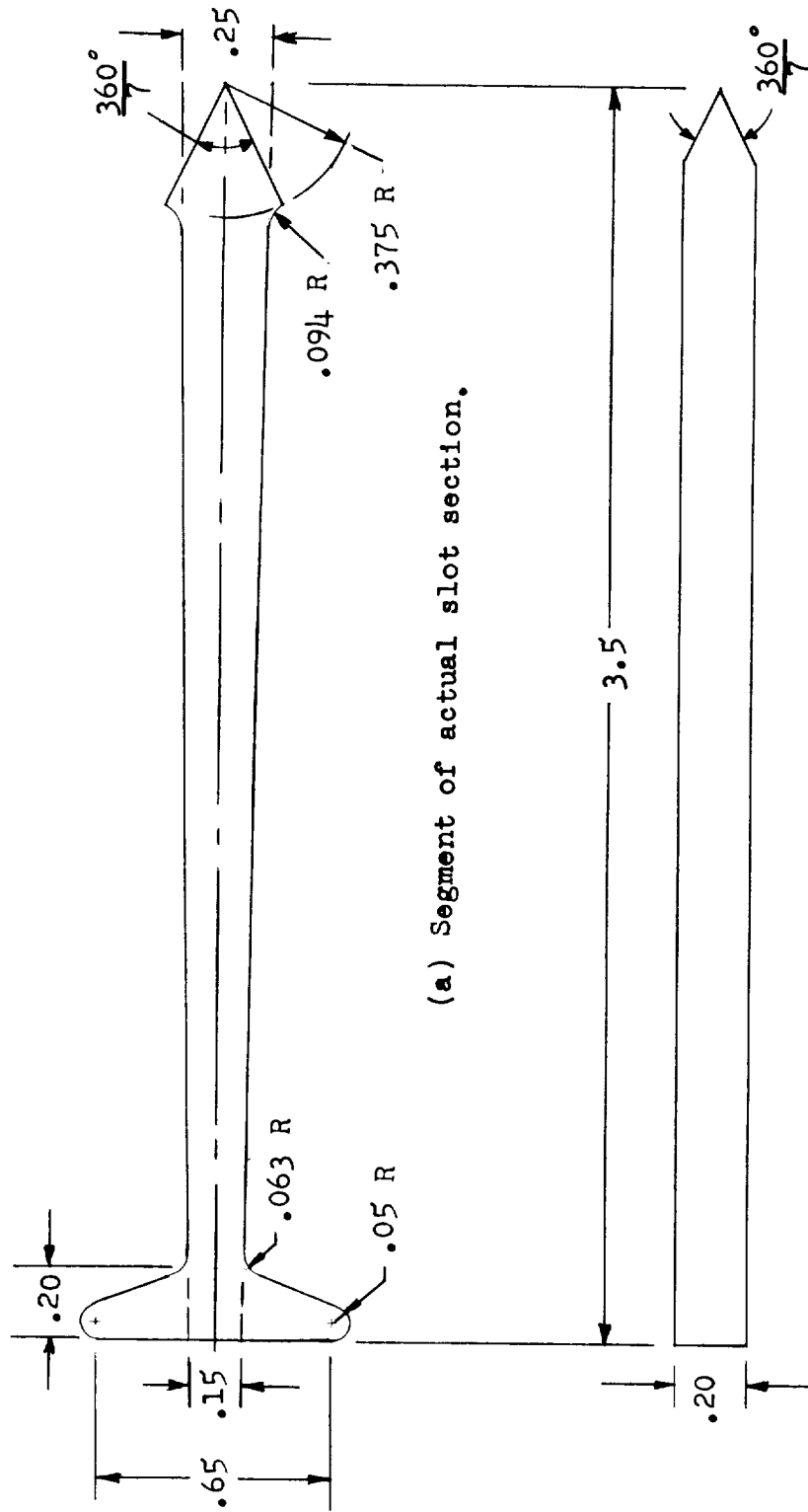
(a) Segment of actual slot section.

360°
7

.20

(b) Segment of assumed slot section.

Figure 10.- Details of actual and assumed slot geometry. All dimensions are in inches.

Longitudinal motor
axis (spin axis)

l_2

b

y

x
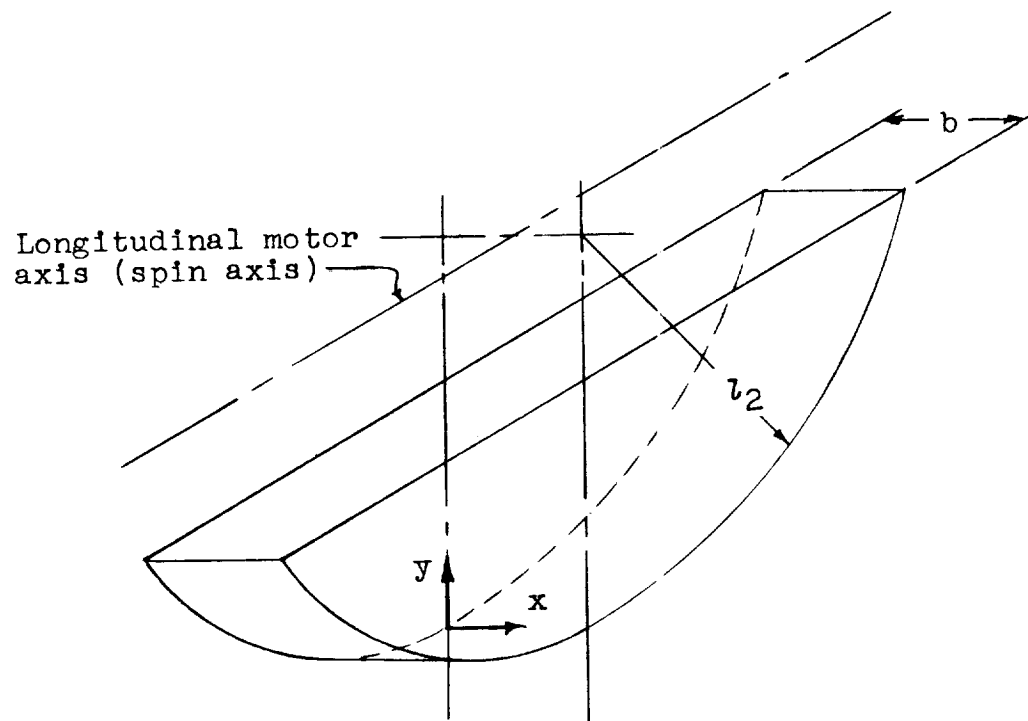
Figure 11.- Three-quarter view of slot geometry at n = 3.
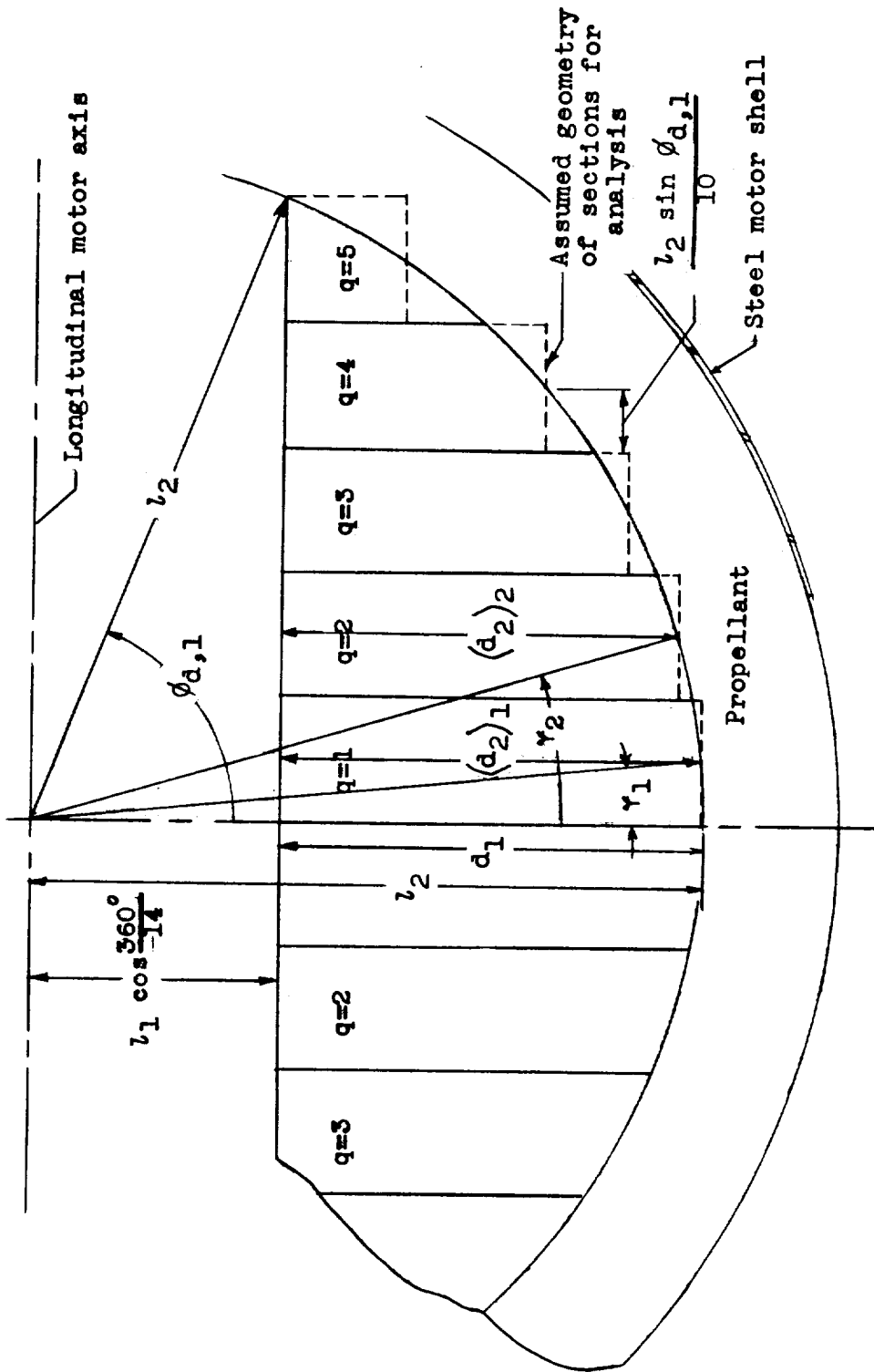
Figure 12.- Side view of slot showing motor geometry at $n = 3$.
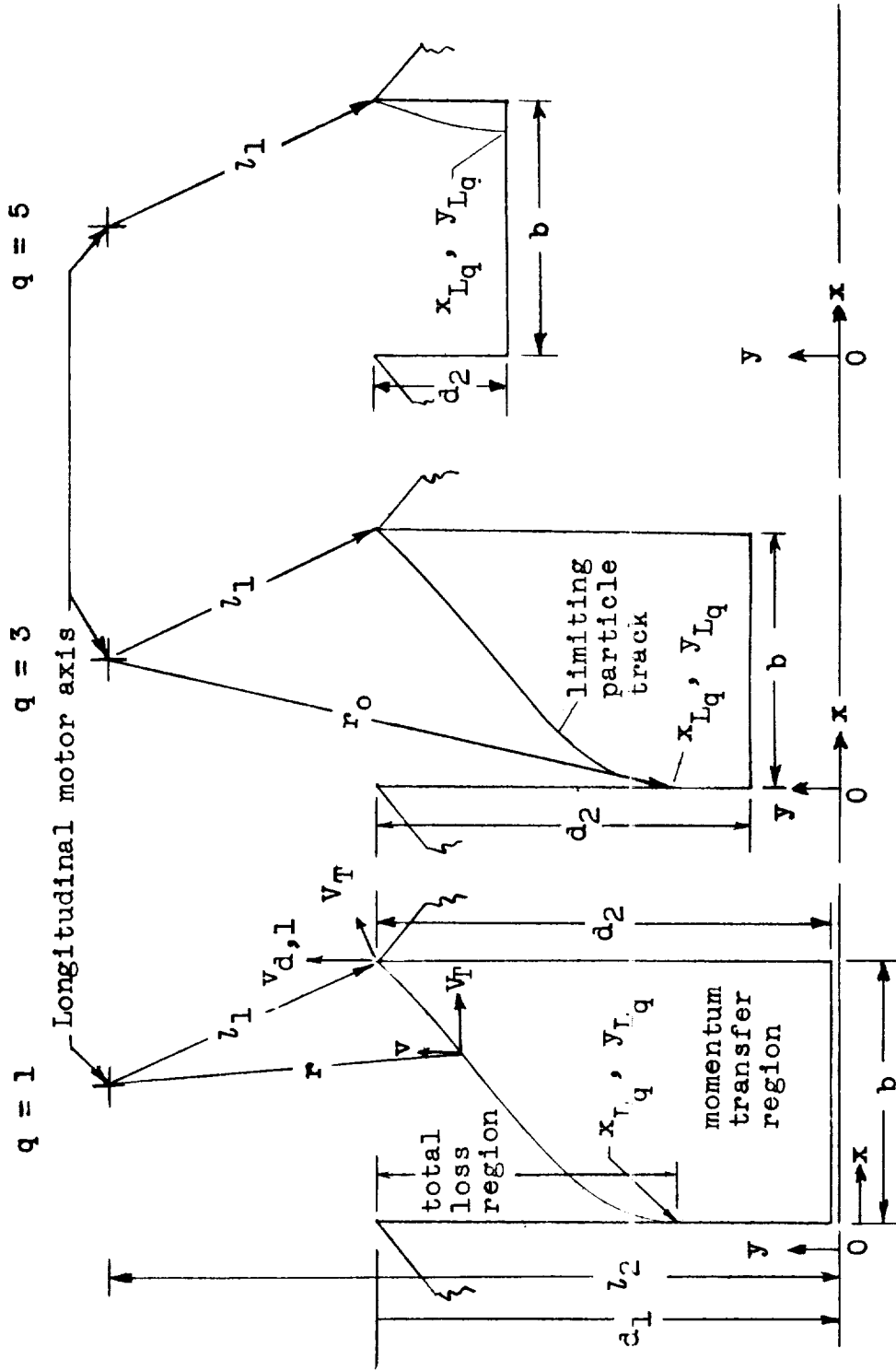
Figure 13.- Slot sections taken perpendicular to motor longitudinal axis. n = 3; q = 1, 3, and 5.

Longitudinal motor axis

Direction of spin
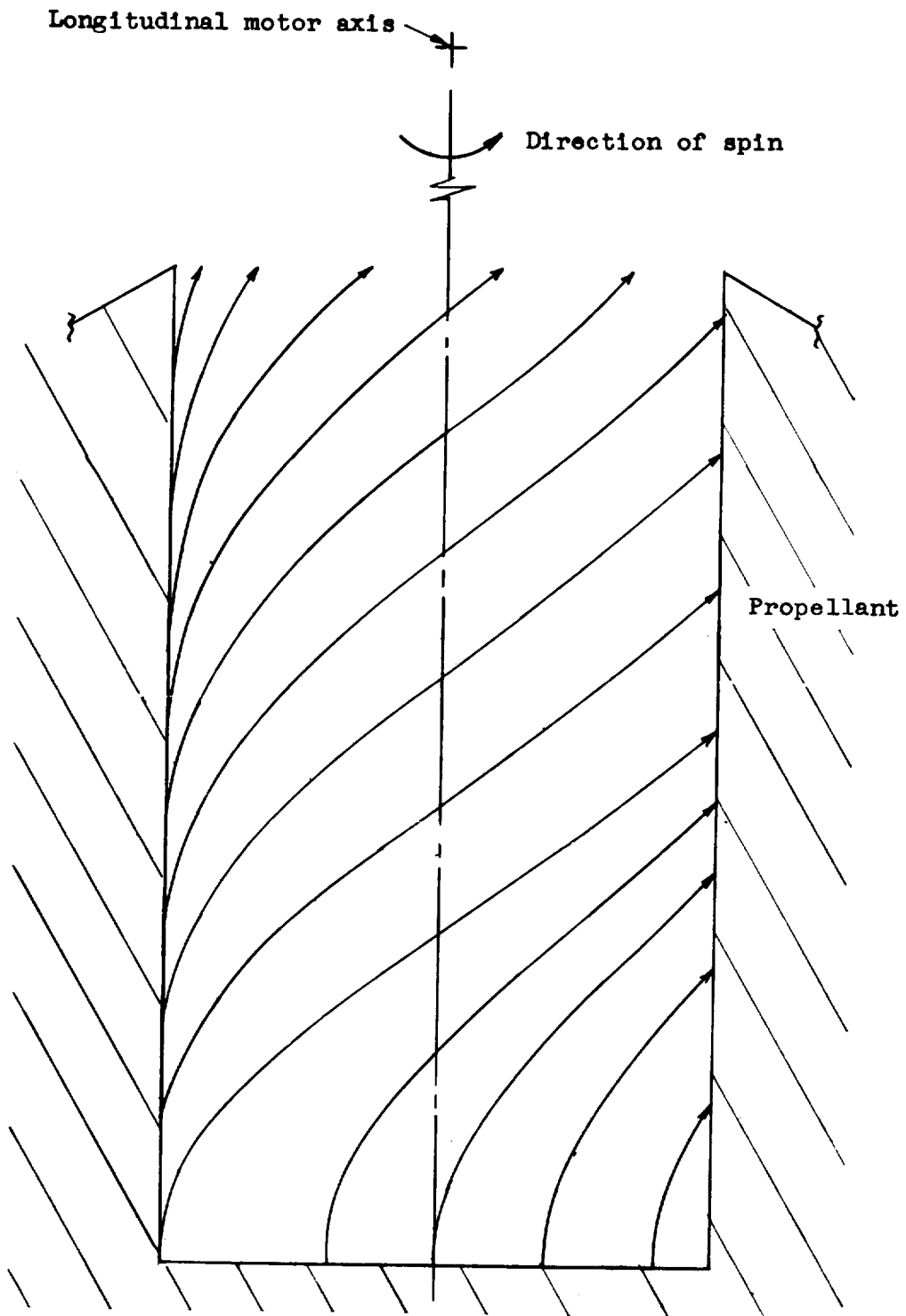
Propellant

Figure 14.- Computed particle flow pattern for q = 1 and n = 3.
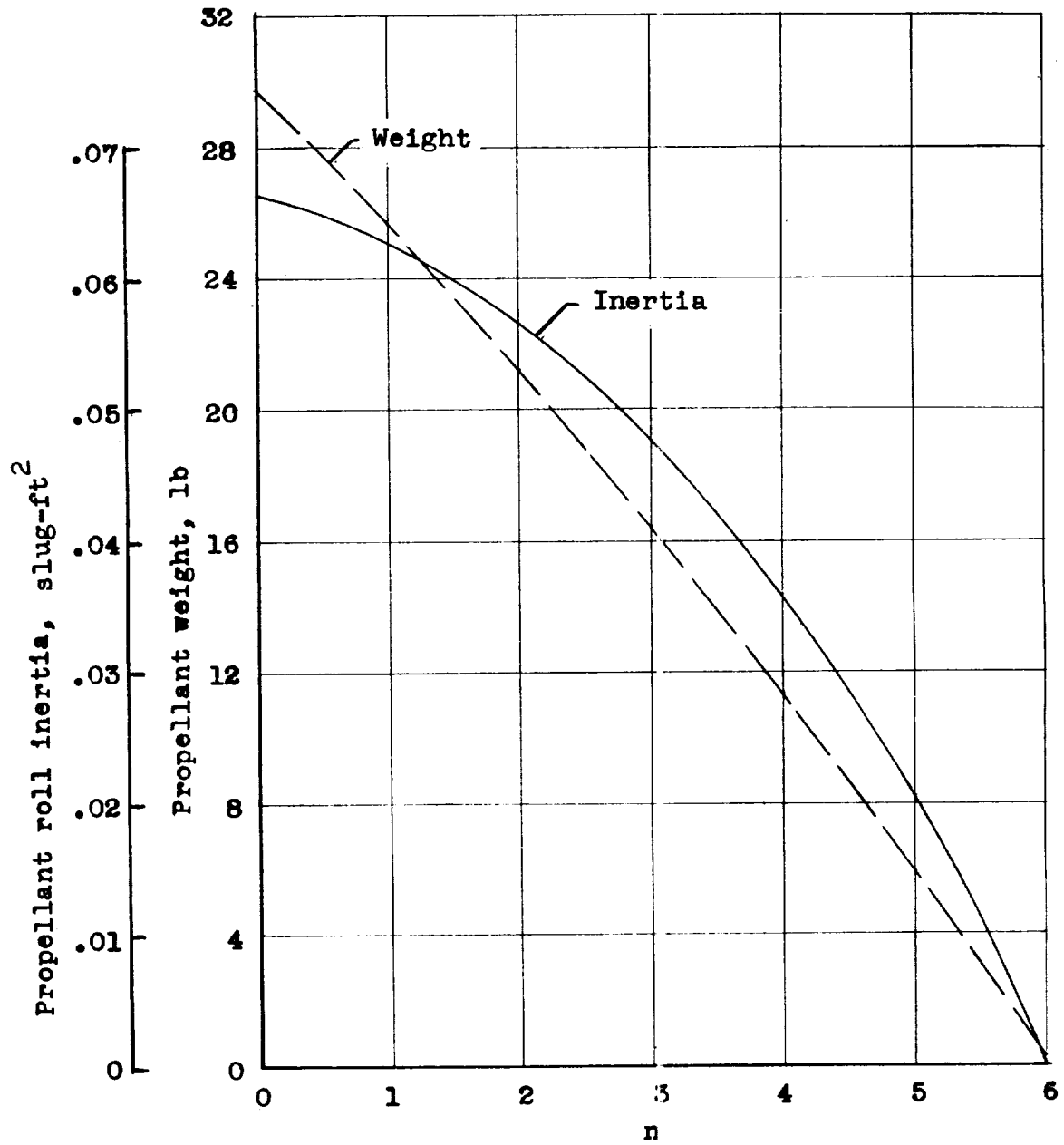
Figure 15.- Calculated variation of weight and roll inertia of propellant during burning. Models 1 and 2.

NASA TM X-75
National Aeronautics and Space Administration.
EXPERIMENTAL AND ANALYTICAL STUDY OF
ROLLING-VELOCITY AMPLIFICATION DURING
THE THRUSTING PROCESS FOR TWO 10-INCH-
DIAMETER SPHERICAL ROCKET MOTORS IN
FREE FLIGHT. C. William Martz and Robert L.
Swain. September 1959. 36p. diagrs., photos., tab.
(NASA TECHNICAL MEMORANDUM X-75)

(Title, Unclassified)

A limited theoretical analysis of spinning-velocity
increase from internal momentum effects is shown to
compare favorably with these experimental results.
Model 1, a heavy-wall motor, experienced an increase
in spin rate during thrusting of about 10 percent,
whereas model 2, a flight-type motor with a lightweight
motor case, experienced an increase of about 19 per-
cent. A simple relationship for "spin-up" which
satisfies the measured results for these models is
reported herein. Both models were ground launched
(over)

Copies obtainable from NASA, Washington

1. Spinning   (1.8.3)
2. Mass and Gyroscopic
   Problems   (1.8.6)
3. Engines, Rocket
                   (3.1.8)
4. Fuel Systems - Engines,
   Rocket   (3.12.1.8)
I. Martz, C. William
II. Swain, Robert L.
III. NASA TM X-75

NASA

NASA TM X-75
National Aeronautics and Space Administration.
EXPERIMENTAL AND ANALYTICAL STUDY OF
ROLLING-VELOCITY AMPLIFICATION DURING
THE THRUSTING PROCESS FOR TWO 10-INCH-
DIAMETER SPHERICAL ROCKET MOTORS IN
FREE FLIGHT. C. William Martz and Robert L.
Swain. September 1959. 36p. diagrs., photos., tab.
(NASA TECHNICAL MEMORANDUM X-75)

(Title, Unclassified)

A limited theoretical analysis of spinning-velocity
increase from internal momentum effects is shown to
compare favorably with these experimental results.
Model 1, a heavy-wall motor, experienced an increase
in spin rate during thrusting of about 10 percent,
whereas model 2, a flight-type motor with a lightweight
motor case, experienced an increase of about 19 per-
cent. A simple relationship for "spin-up" which
satisfies the measured results for these models is
reported herein. Both models were ground launched
(over)

Copies obtainable from NASA, Washington

1. Spinning   (1.8.3)
2. Mass and Gyroscopic
   Problems   (1.8.6)
3. Engines, Rocket
                   (3.1.8)
4. Fuel Systems - Engines,
   Rocket   (3.12.1.8)
I. Martz, C. William
II. Swain, Robert L.
III. NASA TM X-75

NASA

NASA TM X-75
National Aeronautics and Space Administration.
EXPERIMENTAL AND ANALYTICAL STUDY OF
ROLLING-VELOCITY AMPLIFICATION DURING
THE THRUSTING PROCESS FOR TWO 10-INCH-
DIAMETER SPHERICAL ROCKET MOTORS IN
FREE FLIGHT. C. William Martz and Robert L.
Swain. September 1959. 36p. diagrs., photos., tab.
(NASA TECHNICAL MEMORANDUM X-75)

(Title, Unclassified)

A limited theoretical analysis of spinning-velocity
increase from internal momentum effects is shown to
compare favorably with these experimental results.
Model 1, a heavy-wall motor, experienced an increase
in spin rate during thrusting of about 10 percent,
whereas model 2, a flight-type motor with a lightweight
motor case, experienced an increase of about 19 per-
cent. A simple relationship for "spin-up" which
satisfies the measured results for these models is
reported herein. Both models were ground launched
(over)

Copies obtainable from NASA, Washington

1. Spinning   (1.8.3)
2. Mass and Gyroscopic
   Problems   (1.8.6)
3. Engines, Rocket
                   (3.1.8)
4. Fuel Systems - Engines,
   Rocket   (3.12.1.8)
I. Martz, C. William
II. Swain, Robert L.
III. NASA TM X-75

NASA

NASA TM X-75
National Aeronautics and Space Administration.
EXPERIMENTAL AND ANALYTICAL STUDY OF
ROLLING-VELOCITY AMPLIFICATION DURING
THE THRUSTING PROCESS FOR TWO 10-INCH-
DIAMETER SPHERICAL ROCKET MOTORS IN
FREE FLIGHT. C. William Martz and Robert L.
Swain. September 1959. 36p. diagrs., photos., tab.
(NASA TECHNICAL MEMORANDUM X-75)

(Title, Unclassified)

A limited theoretical analysis of spinning-velocity
increase from internal momentum effects is shown to
compare favorably with these experimental results.
Model 1, a heavy-wall motor, experienced an increase
in spin rate during thrusting of about 10 percent,
whereas model 2, a flight-type motor with a lightweight
motor case, experienced an increase of about 19 per-
cent. A simple relationship for "spin-up" which
satisfies the measured results for these models is
reported herein. Both models were ground launched
(over)

Copies obtainable from NASA, Washington

1. Spinning   (1.8.3)
2. Mass and Gyroscopic
   Problems   (1.8.6)
3. Engines, Rocket
                   (3.1.8)
4. Fuel Systems - Engines,
   Rocket   (3.12.1.8)
I. Martz, C. William
II. Swain, Robert L.
III. NASA TM X-75

NASA

NASA TM X-75

from the NASA Wallops Station and were spin sta-
bilized in flight.

NASA

Copies obtainable from NASA, Washington

NASA TM X-75

from the NASA Wallops Station and were spin sta-
bilized in flight.

NASA

Copies obtainable from NASA, Washington